Journal of Hydrology 634 (2024) 131043

Contents lists available at ScienceDirect

Journal of Hydrology

journal homepage: www.elsevier.com/locate/jhydrol

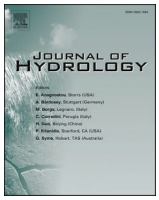

Research papers

Urban pluvial flood modelling in the absence of sewer drainage network data: A physics-based approach

C. Montalvo [a,*], J.D. Reyes-Silva [b], E. Sañudo [a], L. Cea [a], J. Puertas [a]

[a] Universidade da Coruña, Water and Environmental Engineering Group, Center for Technological Innovation in Construction and Civil Engineering (CITEEC), Campus de Elviña, 15071 A Coruña, Spain
[b] TU Dresden, Department of Hydrosciences, Institute for Urban Water Management, 01069 Dresden, Germany

ARTICLE INFO

This manuscript was handled by Yuefei Huang, Editor-in-Chief, with the assistance of Giuseppe Brunetti, Associate Editor

Keywords:
Urban pluvial flooding
Dual models
Iber
SWMM
Data scarcity

ABSTRACT

1D/2D dual drainage models have become one of the most useful tools in the study of urban pluvial floods. However, such models require information about the sewer network that is not always readily available. In this study we present a physics-based approach for assessing urban pluvial floods, with the aim of overcoming the common situation of having limited information on the sewer system. The method proposed involves the use of available open-access information within a virtual sewer network generation tool. This realistic approach allows for the implementation of 1D/2D dual drainage models, such as the recently developed Iber-SWMM model. Results obtained from four storm events using a virtual sewer network in Iber-SWMM were compared with those derived using data from the actual sewer network in a coastal town located in NW Spain. These results revealed that the proposed approach can reasonably represent the sewer network's drainage capacity during pluvial floods, especially compared to other simplified approaches, like the rainfall reduction method. The proposed approach also accounts for the sewer network transport capacity and the impact of overflows when a sewer's capacity is exceeded. Hence the study confirms the significant effect of these processes on the magnitude of pluvial flooding in urban areas. The methodology is shown to be robust, and can be applied to any urban settlement in which no proper record of the sewer network is available.

1. Introduction

Urban pluvial floods often occur due to very intense and short precipitation events, leading to an overload of the sewer network and resulting in physical, economic, and even human losses (Falconer et al., 2009; Jiang et al., 2018; Reyes-Silva et al., 2023; Rosenzweig et al., 2018). Thus far, pluvial floods have received less attention than fluvial or coastal flooding (Prokić et al., 2019; Tanaka et al., 2020), partly because pluvial flooding is far more complicated to evaluate and forecast than fluvial flooding. Numerical models for pluvial flooding are more complex, the required input data is more comprehensive (including in many cases complicated and poorly documented sewer networks), and flood hazard evaluation and forecast is far more sensitive to the spatial and temporal resolution of rainfall. The result of a pluvial flood event depends to a great extent on how the sewer network reacts to rainfall. In addition, the risk of pluvial flooding is expected to rise across Europe over forthcoming years due to a combination of climate change, which is expected to lead to more frequent and intense rainfall events (IPCC, 2014), and new urban developments, which will increase the amount of impervious land (Kaspersen et al., 2017). Indeed, a rise in the frequency of flood impacts over recent years as a result of both these factors has already been reported (Xing et al., 2022). In light of this, most of the flood management plans that will be developed in the immediate future will have to include estimations and measures of potential flood events to mitigate and manage pluvial flood hazard.

To adequately address this hazard, effective methods are needed to estimate the scale and impact of pluvial flood events and to develop mitigation strategies (Reyes-Silva et al., 2023). Hydrodynamic models have become one of the most useful tools here (Xing et al., 2022). Today, 1D/2D dual drainage models are the optimal choice for this kind of analysis, enabling modelers to obtain more realistic results (Chen et al., 2016; Djordjević et al., 1999; Leandro et al., 2009; Martins et al., 2017). Such models solve the two-dimensional shallow water equations on the surface (major drainage system) while maintaining a one-dimensional approach in the sewer network (minor drainage system), allowing for a flow interchange between the two drainage systems (Fraga et al.,

* Corresponding author.
E-mail address: carlos.montalvo@udc.es (C. Montalvo).

https://doi.org/10.1016/j.jhydrol.2024.131043
Received 13 November 2023; Received in revised form 16 February 2024; Accepted 27 February 2024
Available online 10 March 2024

2017; Martins et al., 2018; Sañudo et al., 2020). However, these models require detailed information about the sewer network, which may not always be readily accessible (Li et al., 2023; Reyes-Silva et al., 2023; Xing et al., 2022). Sewer network spatial layout, geometric, and hydraulic characteristics data storage and preparation are the basis of any kind of analysis related to sewers, such as model implementation. However, the quality of information is questionable due to several factors, such as collection practices or input errors. It is estimated that between 25 % and 50 % of network information could be discarded for any kind of analysis (Caradot et al., 2018; Khaleghian & Shan, 2023; Salman & Salem, 2012).

Consequently, in cases of limited data availability, simplified approaches have been devised to account for the sewer network's drainage capacity (SNDC) within 2D models. These approaches include the rainfall reduction method, which involves removing a rate of rainfall from the input precipitation data, or the equivalent infiltration method, which increases rainfall losses in the urban zones (Li et al., 2023; Wang et al., 2018; Xing et al., 2022). These approaches undoubtedly lack a robust and realistic physical basis, in that they assume a constant and spatially uniform drainage capacity over the urban area. Moreover, they cannot consider the overflow returned to the surface through manholes when the sewer network capacity is exceeded, thus ignoring all the complexity of hydraulic processes within the sewer network.

In this context, the main aim of the present study is to develop a physics-based approach for assessing urban pluvial floods, as a means of overcoming the frequently arising issue of limited information on the sewer system. The proposed method involves the use of available open-access information to automatically generate a virtual sewer network (Reyes-Silva et al., 2023) that can then be used in any 1D/2D dual drainage model, such as the recently developed Iber-SWMM model (Sañudo et al., 2020), which will be used here. The results obtained using a virtual sewer network in Iber-SWMM were compared with those derived from a 1D/2D model using data from the actual sewer network in a coastal town located in NW Spain. This comparison revealed that the proposed approach can reasonably represent the SNDC during pluvial floods, improving the predictions obtained with other simplified methods, when the geometry of the real network is unknown. Consequently, it allows for a realistic identification of areas susceptible to pluvial flooding, regardless of the availability of sewer network information.

2. Materials and methods

2.1. Case study

The study area is the coastal urban settlement of Sada, located in NW Spain, one of the rainiest regions in the country. The urban settlement covers approximately 0.6 km^2 and has been identified as an Area of Potential Significant Flood Risk (APSFR) (AdG, 2019) due to having experienced several flooding events in recent years, such as those recorded in March 2016 and December 2022. The urban area is located at the confluence of the rivers Rego Maior and Regato de Fontoira (Fig. 1.a). Right at the confluence the river enters into a culvert box, which extends until it reaches the sea. Thus, sea level exerts an influence on the water surface elevation in the river. The zone receives a substantial amount of runoff, mostly from two highly impermeable areas: the urban area itself and an industrial park located at the headwaters of the basin.

The basin has an area of 24.75 km^2 (Fig. 1.a), with a topography ranging from 255 to 0 m above sea level. The predominant land uses are forest, crops and urban. The study area features a combined sewer system with 11 km of network covering the main urban areas, with multiple outfalls in the culvert box (Fig. 1.b). This area was selected for analysis due to its flooding history, and the availability of real sewer network data, including information on the real sewer layout and hydraulic characteristics of the conduits. This data is essential for validating the approach results. In addition, there is a water level gauge station located at the final section of the river Regato de Fontoira, which can be used for comparisons with the predictions of the model.

2.2. 1D/2D hydrodynamic dual drainage model Iber-SWMM

Iber is a two-dimensional numerical model for simulating free-surface flow and transport processes in unsteady conditions (Bladé et al., 2014). Its hydrodynamic module solves the 2D shallow water equations using an unstructured finite volume solver over a computational mesh, which includes a specific numerical scheme for hydrological applications, calculating rainfall-runoff (hydrological) and inundation (hydraulic) processes simultaneously (Cea & Bladé, 2015). The mass and momentum conservation equations solved by the model can be expressed as follows:

$$\frac{\partial h}{\partial t}+\frac{\partial q_x}{\partial x}+\frac{\partial q_y}{\partial y}=R-i \tag{1}$$

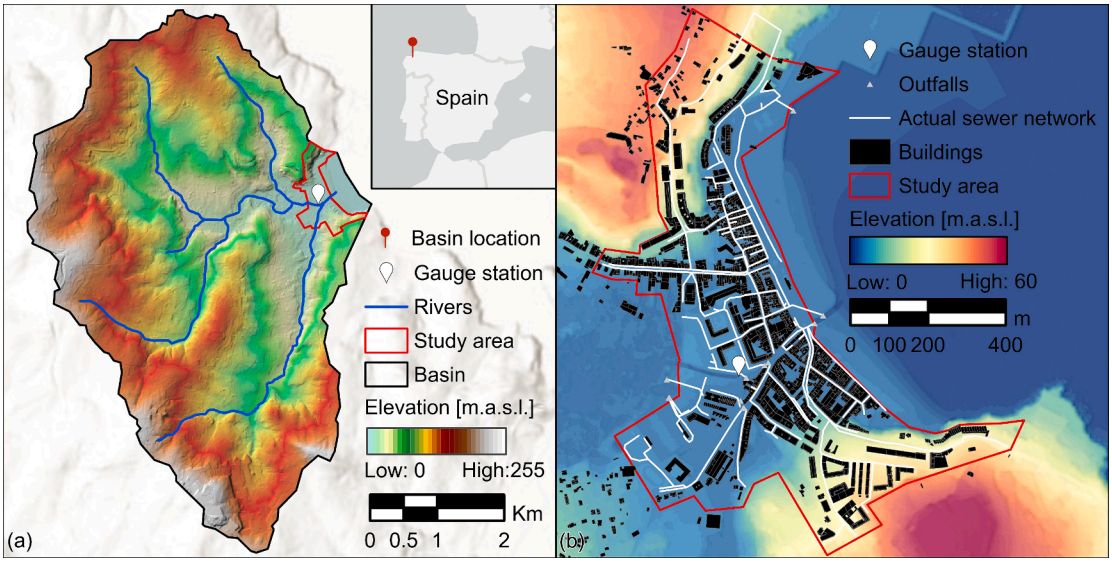

Fig. 1. Digital elevation model from the study basin (a), and the study area (b).

$$\frac{\partial q_x}{\partial t}+\frac{\partial}{\partial x}\left(\frac{q_x^2}{h}+g\frac{h^2}{2}\right)+\frac{\partial}{\partial y}\left(\frac{q_x q_y}{h}\right)=-gh\frac{\partial z_b}{\partial x}-g\frac{n^2}{h^{7/3}}|q|q_x \quad (2)$$

$$\frac{\partial q_y}{\partial t}+\frac{\partial}{\partial x}\left(\frac{q_x q_y}{h}\right)+\frac{\partial}{\partial y}\left(\frac{q_y^2}{h}+g\frac{h^2}{2}\right)=-gh\frac{\partial z_b}{\partial y}-g\frac{n^2}{h^{7/3}}|q|q_y \quad (3)$$

where h is the water depth, q_x, q_y and $|q|$ are the two components of the unit discharge and its modulus, z_b is the bed elevation, n is the Manning coefficient, g is the gravity acceleration, R is the rainfall intensity, and i is the infiltration rate. Iber includes several formulations to compute infiltration losses. In the current study, the Soil Conservation Service Curve Number (SCS-CN) was used. Those equations, and their specific implementation in Iber, have been extensively tested and applied to compute surface runoff at the catchment scale during flood events (Cea et al., 2022; García-Alén et al., 2023; Moral-Erencia et al., 2021; Sanz-Ramos et al., 2021).

EPA SWMM (Storm Water Management Model) is a 1D dynamic sewer network model developed for simulating water flow conveyance within drainage systems. SWMM solves the 1D Saint-Venant equations for gradually varied, unsteady flow (Rossman, 2015). SWMM includes a dynamic link library (DLL) that allows for the retrieval and setting of hydraulic variables with other models during the simulation. It was recently coupled with Iber to obtain the 1D/2D dual drainage model Iber-SWMM (Sañudo et al., 2020).

The surface and sewer network equations are computed independently by each model. However, water exchange between models occurs at every synchronization time step, ensuring a correct coupling and also maintaining the mass balance of water. Interaction between the overland flow and the sewer drainage system is limited to inlets and manholes. Surface water can enter the sewer network only through the inlets, while the water can only return to the surface through manholes (Sañudo et al., 2020). Additionally, rainfall discharges on the roofs of building are computed using a subcatchment approach by solving a nonlinear reservoir equation (Sañudo et al., 2022).

2.3. Virtual sewer network generation and dimensioning tool

This is a spatial tool that allows for the generation of a realistic virtual sewer network, based on open-access information and conforming to local drainage network constraints. The tool was developed in a geographic information system (GIS) environment, utilizing the Python console within the QGIS software (Reyes-Silva et al., 2023).

The tool defines a realistic network topology by assuming that the layout of the sewer network and of the streets are similar, based on the high degree of correlation between roads and urban water infrastructure (Mair et al., 2017). This layout is determined by considering all the streets within a defined study area that are connected to a possible outfall. Manholes are located at the points where streets start or intersect with each other. To define the minimum number of conduits connecting any manhole to the outlet point, a minimum spanning tree configuration is determined using Kruskal's algorithm (Kruskal, 1956; Reyes-Silva et al., 2023).

Manhole invert elevations are calculated from the Digital Elevation Model (DEM) as the difference between the ground elevation and a user-defined node depth that can be established based on local design guidelines. The tool performs an evaluation and correction, if needed, of these elevations in order to ensure a gravitational flow towards the network outlet (Reyes-Silva et al., 2023).

For each conduit, two inflows are defined: the stormwater flow, determined by several synthetic design storm parameters that include user-defined return period, intensity, and duration; and the wastewater flow, calculated based on user-defined data such as population density, Land Registry, and daily per capita water consumption. Subsequently, conduit diameters are calculated through an iterative process, in accordance with local design guidelines, in order to ensure the adequate performance of the sewer network under the specified design flow conditions. The tool is capable of designing both separate and combined sewer system schemes (Reyes-Silva et al., 2023).

The original tool is not capable of generating the layout of inlets (Reyes-Silva et al., 2023). Since the location of inlets is necessary in Iber-SWMM to couple the major and minor drainage systems, a complementary GIS routine was developed to generate the location of inlets based on the street network layout and in accordance with local sewer network design guidelines, as other authors have also done (Bertsch et al., 2017). For this purpose, the inlet layout was defined based on two conditions: that the inlets are located near street intersections, and that they are spaced at no more than a maximum distance apart, as defined in local regulations. The GIS routine generates inlets with the defined maximum spacing and following the street network layout, with random displacements of up to 3 m from the street axis.

2.4. Rainfall events

The study area has suffered frequent pluvial flooding events over recent years. Two of the most significant flood events took place in December 2022 (E1) and March 2016 (E2), both of which were used here to analyze the proposed approach. The event of December 2022 was also used to calibrate the model. Raster fields of precipitation with a spatial resolution of 250 m and a time resolution with data every hour, provided by the regional meteorological agency (MeteoGalicia), were used as inputs for Iber's hydrological module. In addition to these two real events, two synthetic design storms with a duration of 24 h and return periods of 10 years (E3) and 100 years (E4) were also considered in the analysis. The key characteristics of these events are set out in Table 1 (See Fig. 2).

2.5. Scenarios

Five different scenarios for representing the SNDC were implemented, and were used to calculate the maximum flood extent for the four rainfall events defined in Table 1.

2.5.1. 1D/2D dual model using the actual sewer network (S1)

This scenario was computed with the coupled model Iber-SWMM using the actual sewer network data available for the study area. Due to a lack of observed information about the spatial extent of the floods, the results obtained for this scenario will be considered as the most realistic for each storm event, and are used as a benchmark for the other four scenarios described below.

2.5.2. 2D overflow model without sewer network (S2)

This scenario was computed with the 2D model Iber, which only computes the overland flow in the major drainage system, without considering the sewer network. The absence of the SNDC effect is sometimes justified by assuming that, under extreme rainfall conditions, the sewer network is overwhelmed and hence it does not have a significant effect on the extent and magnitude of pluvial floods, or simply assuming that the results obtained are conservative in terms of flood hazard (Schmitt and Scheid, 2020). The results from this scenario were compared with the results obtained in S1 in order to estimate the effect of the SNDC in the flood extent.

2.5.3. 2D overflow model with rainfall reduction for sewer network representation (S3)

This scenario is numerically similar to S2 but a given rainfall rate is removed from the input precipitation. The reduction in the rainfall rate is intended to represent the SNDC, and therefore only the 2D overland flow generated by the precipitation excess is modelled. The volume of the precipitation removed is equal to the volume used for the design of the sewer network (Wang et al., 2018). In this case, the volume of a design storm with a duration of 24 h and a 2-year return period was

Table 1
Key hydrometeorological characteristics of the analyzed events.

Rainfall event	Duration (days)	Max rain rate in 1 hour (mm/h)	Total accumulated rainfall (mm)	Max sea level (m)	Hyetograph
E1: December 2022	3	12.3	118.8	2.20	Fig. 2.a
E2: March 2016	3	6.2	114.5	1.48	Fig. 2.b
E3: T10	1	23.1	77.6	2.00	Fig. 2.c
E4: T100	1	36.0	120.9	2.20	Fig. 2.d

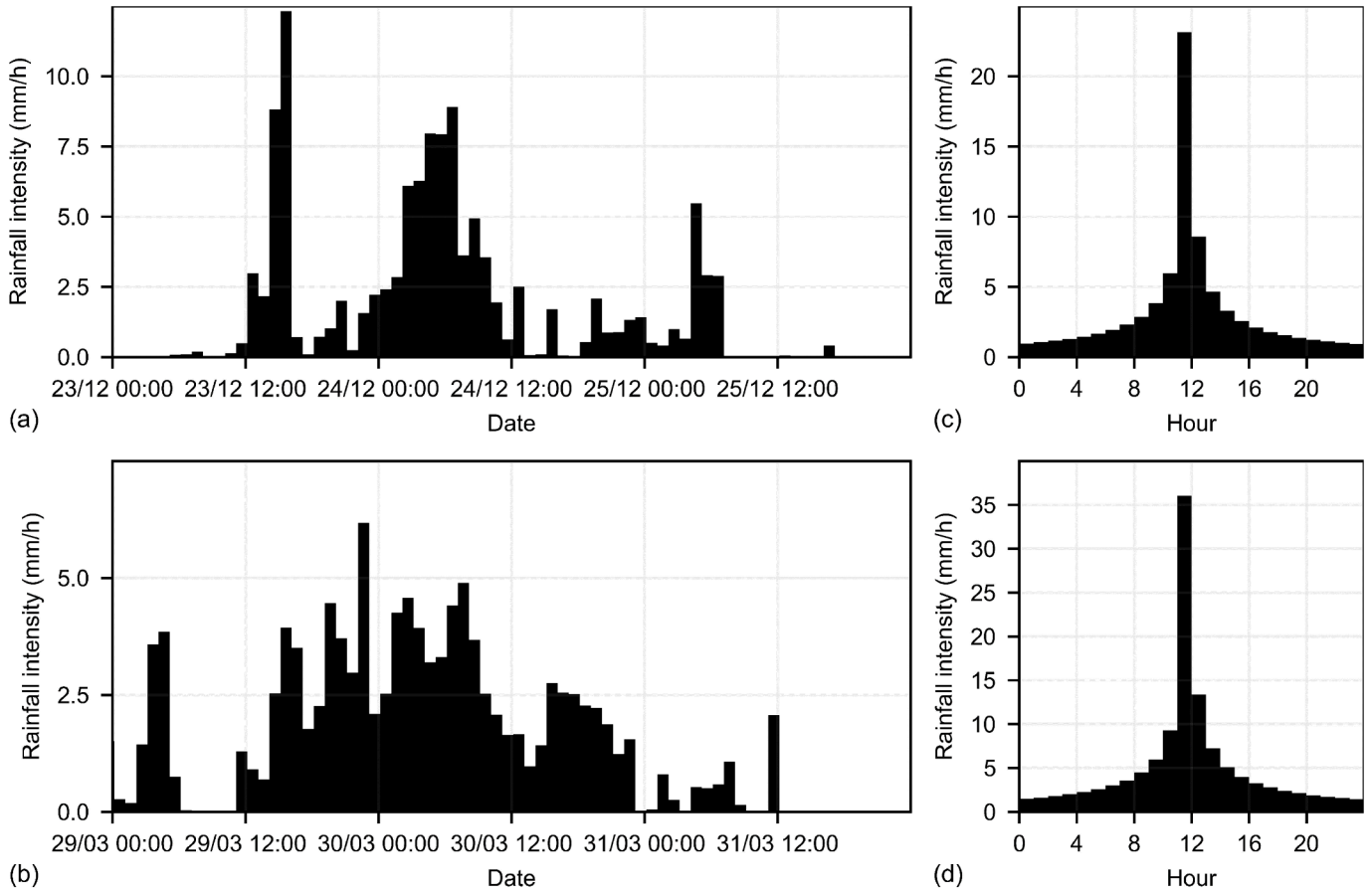

Fig. 2. Rainfall hyetographs of the analyzed events: December 2022 (a), March 2016 (b), design storms with a duration of 24 h and return periods of 10 years (c) and 100 years (d).

removed at a constant rate from the gross precipitation.

2.5.4. 1D/2D dual model using a virtual sewer network (S4)

This scenario was computed with the coupled model Iber-SWMM, as in the case of S1. However, instead of using the actual sewer network, a realistic virtual sewer network was implemented in the model, this obtained using the approach of Reyes-Silva et al. (2023), described above in Section 2.3. The comparison of the results obtained in scenarios S1 and S4 allows us to assess whether the virtual sewer network is a valid alternative means of representing the SNDC in the absence of real sewer network information.

2.5.5. 2D overflow model using a virtual inlet layout (S5)

This scenario is a simplification of S4 that only uses a realistic representation of the inlet layout, obtained using the methodology described in Section 2.3, without any other definition of the sewer network. The inlets are only used in the model to account for the capacity of the sewer network to infiltrate runoff from the surface to the conduits, but the flow on these is not computed. Therefore, this scenario is computed using only the 2D overland flow model, and does not consider the overflow to the surface through manholes when the sewer network capacity is exceeded.

2.6. Model setup

The numerical model built using Iber-SWMM had an unstructured mesh with 467,162 triangular elements of different sizes. The mesh is coarser in the hillslopes (30 m), more defined on the coastal borderline and in the industrial park (10 m), and finer in both the study area (2 m) and the main water streams such as rivers, channels, and culvert boxes (1 m) (Fig. 3). The sea level was defined as a boundary condition at the coastal front (Fig. 3.b). In the real rainfall events, E1 and E2, the sea level at the boundary was defined from the sea level time series registered at a local tidal gauge. In the synthetic rainfall events, E3 and E4, the sea level was considered as a constant value. The maximum sea level for each event is shown in Table 1. The terrain elevation at each mesh vertex was interpolated from a 2 m resolution DEM at the basin scale (Fig. 1.a), and from a 20 cm resolution LiDAR-derived DEM within the study area (Fig. 1.b). In order to keep the model simple and to focus the analysis on modelling the effect of the sewer network, only two Manning coefficients were used to represent terrain roughness, associated respectively with the hillsides and the main water streams. While this

Fig. 3. SCS-CN values in the whole catchment (a), SCS-CN values in the study area (b), and detail of the numerical grid within the study area (c).

assumption might be an oversimplification of the bed roughness parametrization, it shouldn't have any relevant effect in the comparison of the different modelling scenarios included in Table 2, since the bed roughness parametrization was the same in all of them, the only difference being the way in which the sewer network is considered in the model.

The spatial distribution of the CN on the hillslopes was obtained from a 250 m resolution SCS-CN map calculated following the methodology developed by Ferrer-Julià (2003). Polygons based on the geometry of soil use maps were defined to manually assign the CN values to the next specific areas, such as the concrete zones (CN = 95) and green areas (CN = 60) within the study area (Fig. 3.b). The main channel of the water streams and the sea bed were assumed to be impervious areas, since in these zones the soil is completely saturated. It was also assumed that whole industrial park (which has a high degree of pavement) was impervious.

2.7. Virtual sewer network for the study area

A single outfall location was defined in order to build the virtual sewer network, in contrast to the multiple outfalls that exist in the actual sewer network (Fig. 1.b). This was done intentionally, to reflect a situation in which knowledge of the network layout is minimal. The required input spatial data required by the virtual sewer generation tool were obtained from a variety of sources: the street network layout was obtained from OpenStreetMaps geodatabase; the 20 cm resolution DEM, the buildings layout, and the population data were obtained from local government data portals. The design storm parameters and guidelines were defined based on the current Spanish regulation "*Norma 5.2 – IC Drenaje Superficial*" (MOPU, 2016).

2.8. Calibration of scenario S1 in storm event E1

The model performance under scenario S1 was assessed using recorded data from a high-intensity precipitation event that occurred over three days, from December 23rd to 26th, 2022 (E1). The simulated time series of water surface elevation were compared with the data recorded at the gauge station located in the study zone (Fig. 1).

Four model parameters were calibrated: a multiplier of the spatial distributed values of SCS-CN values (Fig. 3) and initial abstractions from the SCS-CN method, as well as the two Manning roughness values associated with the hillsides and the water bodies as rivers and channels. The calibration process was performed manually, through trial and error, using a qualitative assessment that involved observing the shape of the resulting hydrograph, and quantitatively by obtaining the Nash-Sutcliffe statistical (NSE) coefficient (Nash & Sutcliffe, 1970).

Due to the lack of detailed spatial observations of the flood extent during the flood event, the spatial results obtained from the simulated maximum inundation map were only compared with press reports released during the week of the storm event. This allowed us to verify whether the streets that experienced flooding during the event matched the streets represented as flooded in the model.

Table 2
Summary of the five scenarios used to represent the SNDC for the analysis.

Scenario	Model	SNDC representation
S1	1D/2D	Actual sewer network
S2	2D	Without sewer network
S3	2D	Rainfall reduction
S4	1D/2D	Virtual sewer network
S5	2D	Virtual inlet layout

2.9. Performance assessment of the SNDC representation

The performance assessment of S3, S4, and S5 was conducted by contrasting the flood extent computed under these scenarios with those of S1, in the four rainfall events analyzed (Table 1). The comparison of the flood extent under the different scenarios was based on three performance indices: the Hit Rate (Ec. 4), that is, the proportion of the area observed as flooded that the model also predicts as flooded; the False Alarm Ratio (Ec. 5), the proportion of the area predicted as flooded by the model that is classified as dry in the observation; and the Critical Success Index (Ec. 6), a commonly used ratio that penalizes both misses and false alarms. For the computation of all these indices the results obtained in S1 were taken as the observed (i.e. real) values. These kinds of cell-by-cell performance indices are commonly used in the context of flood modelling (Bennett et al., 2013; Cea et al., 2022; Grimaldi et al., 2016; Wang et al., 2018) and are evaluated thus:

$$HR = \frac{TP}{TP + FN} \tag{4}$$

$$FAR = \frac{FP}{TP + FP} \tag{5}$$

$$CSI = \frac{TP}{TP + FP + FN} \tag{6}$$

where HR is the Hit Rate, FAR is the False Alarm Ratio, CSI is the Critical Success Index, TP are the true positives (number of cells correctly predicted as flooded), FP are the false positives (number of cells incorrectly predicted as flooded), and FN are the false negatives (number of cells incorrectly predicted as dry) (Table 3). The HR and CSI scores vary

Table 3
Contingency table for the evaluation of water depth predictions.

	Observed as flooded	Observed as dry
Predicted as flooded	TP (True positive)	FP (False positive)
Predicted as dry	FN (False negative)	TN (True negative)

between 0 (worst performance) and 1 (best performance), while the FAR varies between 0 (best performance) and 1 (worst performance). A cell is considered to be predicted as flooded if the water depth computed by the numerical model is greater than 0.10 m.

3. Results and discussion

3.1. Virtual sewer network layout

The virtual sewer network generated using the tool developed by Reyes-Silva et al. (2023) is consistent with the real sewer network (Fig. 4). Hence, the hypothesis regarding the correlation between the sewer network layout and the street network layout seems to be validated. However, the virtual network has fewer elements than the real one (Table 4), which can be attributed to the parameters defined in the virtual sewer network generation tool as the minimum number of conduits connecting any manhole to the outlet point or the separation between elements, these having been defined based on the actual design guidelines. Nevertheless, it covers nearly the same geographical area as the real network (Fig. 4).

Differences in the diameter of the conduits are also observed in some sections of the network (Table 4). This can be attributed to two factors: first, the virtual network has a lower number of conduits; and second, we assumed a single outfall location (Fig. 4). As a result of this, there are sections of the virtual network that carry a higher flow than the real network, hence requiring larger diameters.

3.2. Calibration of scenario S1 in storm event E1

After calibrating the numerical model with the water elevation data registered at gauge station S1 during event E1 (Fig. 5), the infiltration related parameters obtained were 0.52 for the SCS-CN multiplier and 0.01 for the initial abstractions multiplier, which is lower than the commonly assumed value of 0.2. Several studies have achieved similar results regarding the initial abstractions when using the SCS-CN losses model (Shi et al., 2009). Regarding the terrain roughness, the Manning coefficients obtained were 0.100 for hillsides and 0.078 for the water streams, both values falling within the common ranges found in the literature (Chow, 1959). Although the later one is quite a high value for a river bed, it is justified by the amount of vegetation present in the stream. With these values, the hydrograph computed at the gauge station in scenario S1 adequately fits the main peak of the observed hydrograph (Fig. 5). Additionally, it responds to all three precipitation pulses that are present in the event. The achieved NSE coefficient is 0.83, which is considered as a good fit according to standards reported in the literature (Ritter & Muñoz-Carpena, 2013) (See Table 5).

Four different zones were defined within the urban area for the evaluation of the flood extent predictions (Fig. 6). The streets Cambre, Culleredo, Abegondo, and La Laguna, located in zone 1, as well as the streets La Laguna, Venezuela, and A Lagoa Alley, located in zone 2 (Fig. 6.a), experienced flooding during E1, according to local press reports. These two zones largely correspond to the flooded areas on the maximum inundation map obtained from S1 (Fig. 6.b). Furthermore, there are no press reports confirming flooding in the Linares Rivas street or La Maraina and Barrié de la Maza avenues, located in zone 3, or a parking lot in zone 4, which were not flooded in the results obtained from S1 either. This is a significant difference from the results of S2, where these areas also appear flooded during E1 (Fig. 6.c).

The previous observations confirm that the results obtained with S1 are realistic, and this model configuration was therefore used as a benchmark for comparisons with the other scenarios in the four analyzed events.

3.3. Scenarios performance assessment

The scenario with the best performance indices for storm event E1 was S4 (Table 6), which accurately represented the real SNDC. The simulated maximum inundation map was quite similar to that obtained with S1, the major difference appearing within zone 2, where the model

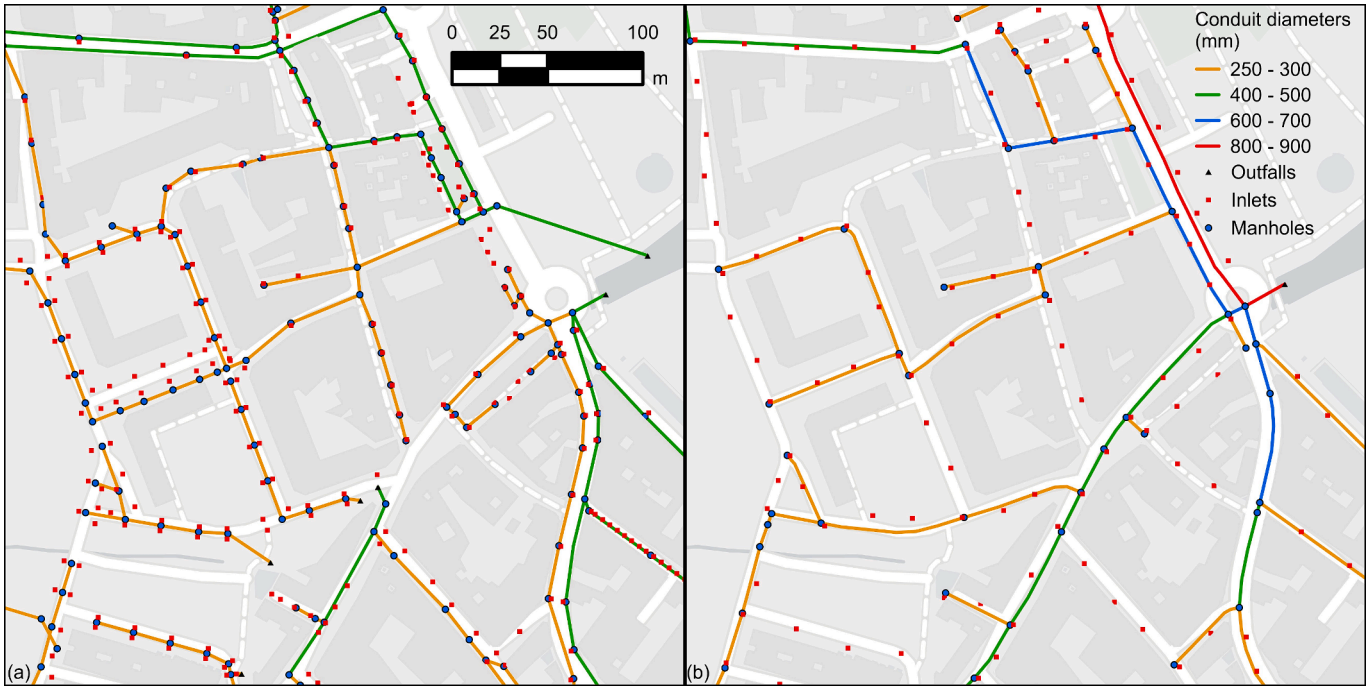

Fig. 4. Real (a) and virtual (b) sewer networks in the study area.

Table 4
Key characteristics of the real and virtual sewer networks in the study area.

Sewer network	Length	Percentage by diameters (mm)				Number of elements		
	(km)	200–300	400–500	600–700	800–900	Outfalls	Manholes	Inlets
Real	11.02	66 %	29 %	5 %	0 %	13	444	516
Virtual	8.57	68 %	21 %	8 %	3 %	1	149	386

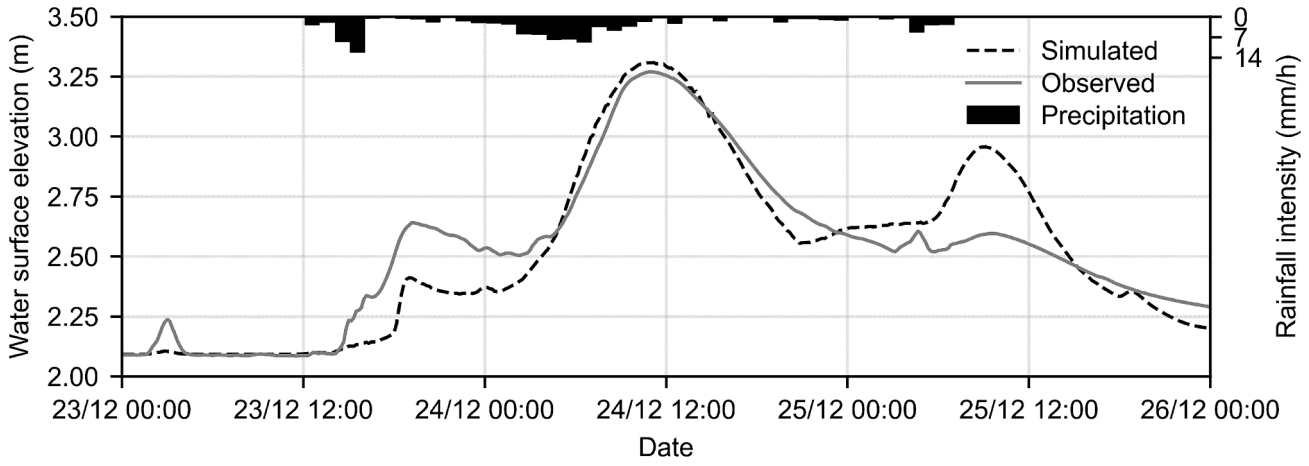

Fig. 5. Simulated and observed hydrographs at the gauge station for S1 during E1.

Table 5
Summary of calibration process.

Parameters Obtained				NSE coefficient
SCS-CN multiplier	Initial abstractions	Manning coefficients for hillsides	Manning coefficients for water streams	
0.52	0.01	0.100	0.078	0.83

slightly overestimated the SNDC effect (Fig. 7.b). Scenario S3 did represent the SNDC in zones 1 and 2, similarly to S4; however, in zones 3 and 4 the results obtained with S3 significantly underestimated the SNDC effect (Fig. 7.a), resulting in high FAR and low CSI values. By contrast, scenario S5 substantially overestimated the SNDC in zones 1 and 2, while it accurately represented the flood extent in zones 3 and 4, resulting in low HR and CSI values.

All three scenarios (S3-S5) overestimated the SNDC in event E2. This produced, for all scenarios, lower HR values than those obtained in event E1. The best performing scenario was again S4, achieving the best

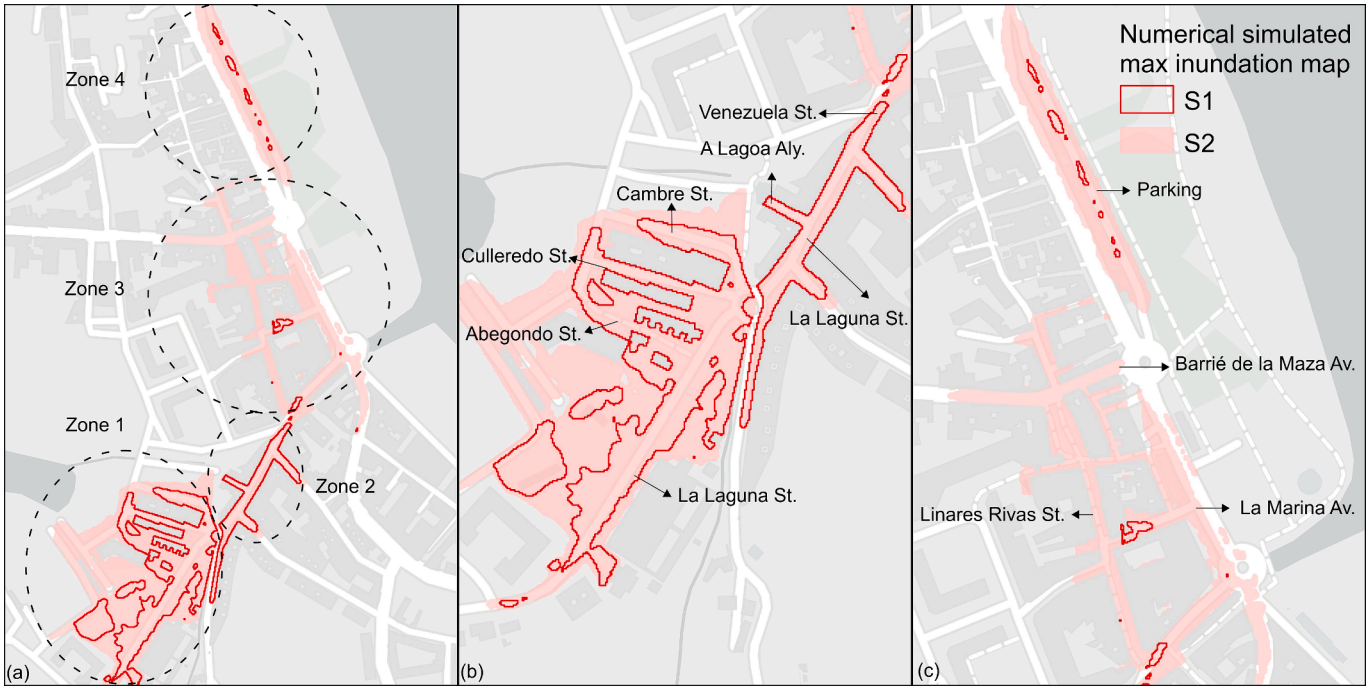

Fig. 6. Study zones (a) and streets (b & c) within numerical simulated maximum inundation maps for S1 and S2 during E1.

Table 6
Flood extent performance indices for scenarios S2, S3, S4 and S5 compared with S1 for the four rainfall events.

	E1				E2				E3				E4			
	S2	S3	S4	S5	S2	S3	S4	S5	S2	S3	S4	S5	S2	S3	S4	S5
HR	1	0.840	0.870	0.500	1	0.705	0.637	0.368	1	0.562	0.810	0.535	1	1	0.913	0.640
FAR	0.547	0.163	0.056	0.005	0.525	0.134	0.009	0.009	0.197	0.058	0.009	0.006	0.687	0.641	0.048	0.006
CSI	0.381	0.560	0.746	0.493	0.252	0.446	0.608	0.355	0.355	0.365	0.745	0.506	0.594	0.610	0.871	0.636

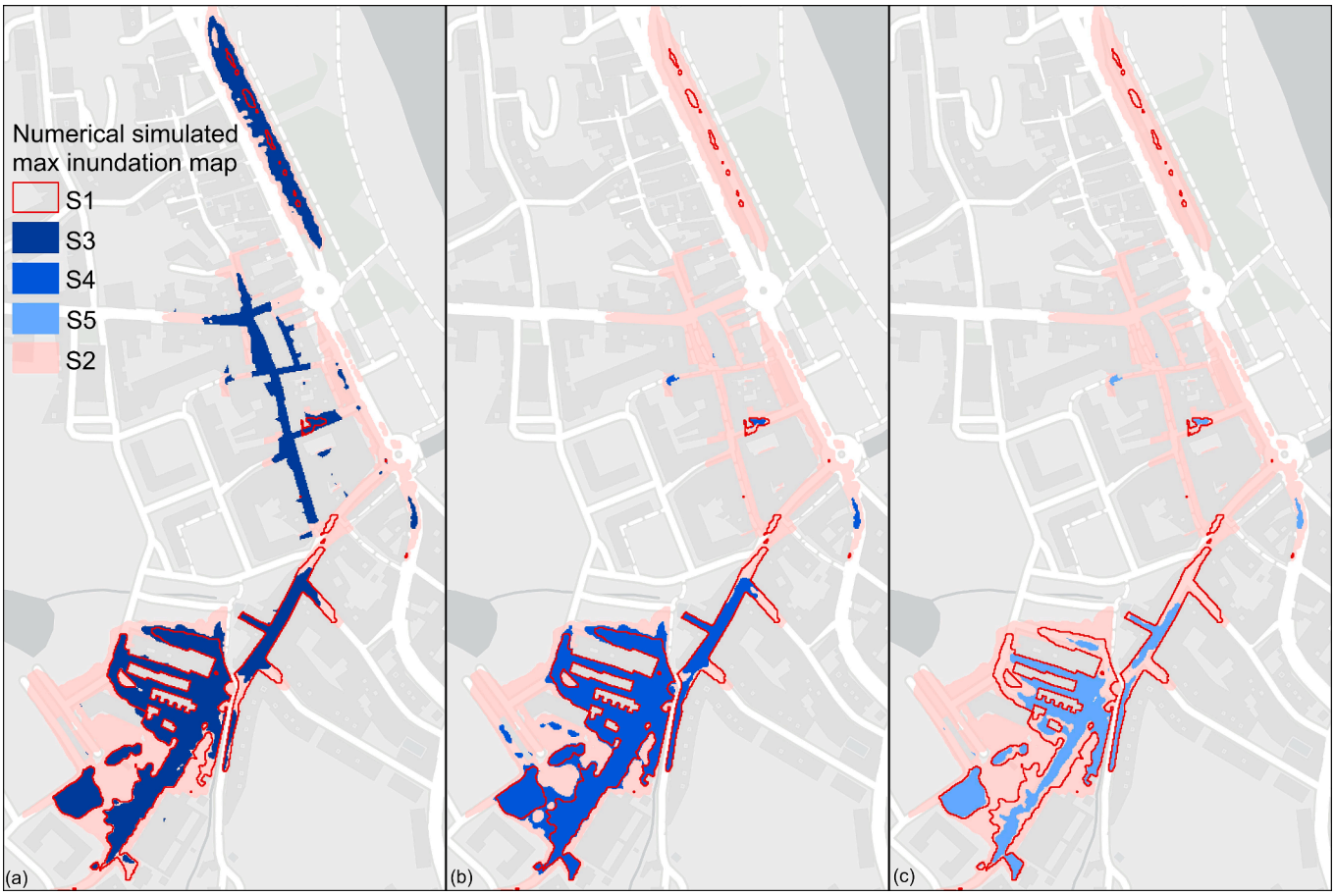

Fig. 7. Numerical simulated maximum inundation extent maps for scenarios S3 (a), S4 (b) and S5 (c) compared with S1 and S2 in the study zones for event E1.

CSI value (0.608), a HR value similar to S3 (0.637), and a FAR as low as S5 (0.009). Despite a slight overestimation of the SNDC in zones 1 and 2 (leading to a smaller inundation extent) the model successfully represented the flood extent in zones 3 and 4 (Fig. 8.b). Scenario S3 had the same problems as S4 in zones 1 and 2, and significantly underestimated the SNDC in zones 3 and 4 (Fig. 8.a). Meanwhile, as was the case in event E1, scenario S5 again produced a significant overestimation of the SNDC in zones 1 and 2 (Fig. 8.c).

In event E3 the simulated maximum inundation maps obtained with scenarios S1 and S4 were quite similar in all four zones (Fig. 9.b), leading to very good performance indices (HR = 0.81, FAR = 0.01 and CSI = 0.75). On the other hand, scenarios S3 and S5 overestimated the SNDC in zone 1 (Fig. 9.c) and, once again, scenario S3 significantly underestimated the SNDC in zones 2, 3 and 4 (Fig. 9.a). Scenario S5 obtained a good FAR value, but at the expense of lower HR and CSI ratios. Meanwhile, scenario S3 obtained poor values of the three performance indices.

Event E4, which is associated with a return period of 100 years, is the one with the highest rainfall intensity and total rainfall depth (Table 1), leading to the largest flood extent. In this event the SNDC seems to be negligible in zones 1 and 2, as the simulated maximum inundation maps were similar for all scenarios except S5, in which the SNDC was significantly overestimated (Fig. 10). The best qualitative and quantitative results are again obtained with S4 (HR = 0.91, FAR = 0.05 and CSI = 0.87), although it overestimated the SNDC in zone 3 (Fig. 10.b). In scenario S3 the SNDC was negligible in all four zones (Fig. 10.a), resulting in significantly high FAR and low CSI values for this scenario. By contrast, S5 substantially overestimated the SNDC in all four zones (Fig. 10.c), resulting in low HR and CSI values.

4. Discussion

4.1. Scenario-based evaluation

The calibrated results obtained with scenario S1 seem to provide a good approximation for representing the pluvial flooding process during the real storm event E1. This served as a valuable starting point for analyzing other intense rainfall events, as well as for evaluating the performance of alternative scenarios.

The comparison of the results obtained with scenarios S1 and S2 highlighted the importance of taking the SNDC into account. In all four events, disregarding the SNDC in S2 led to an overestimation of the

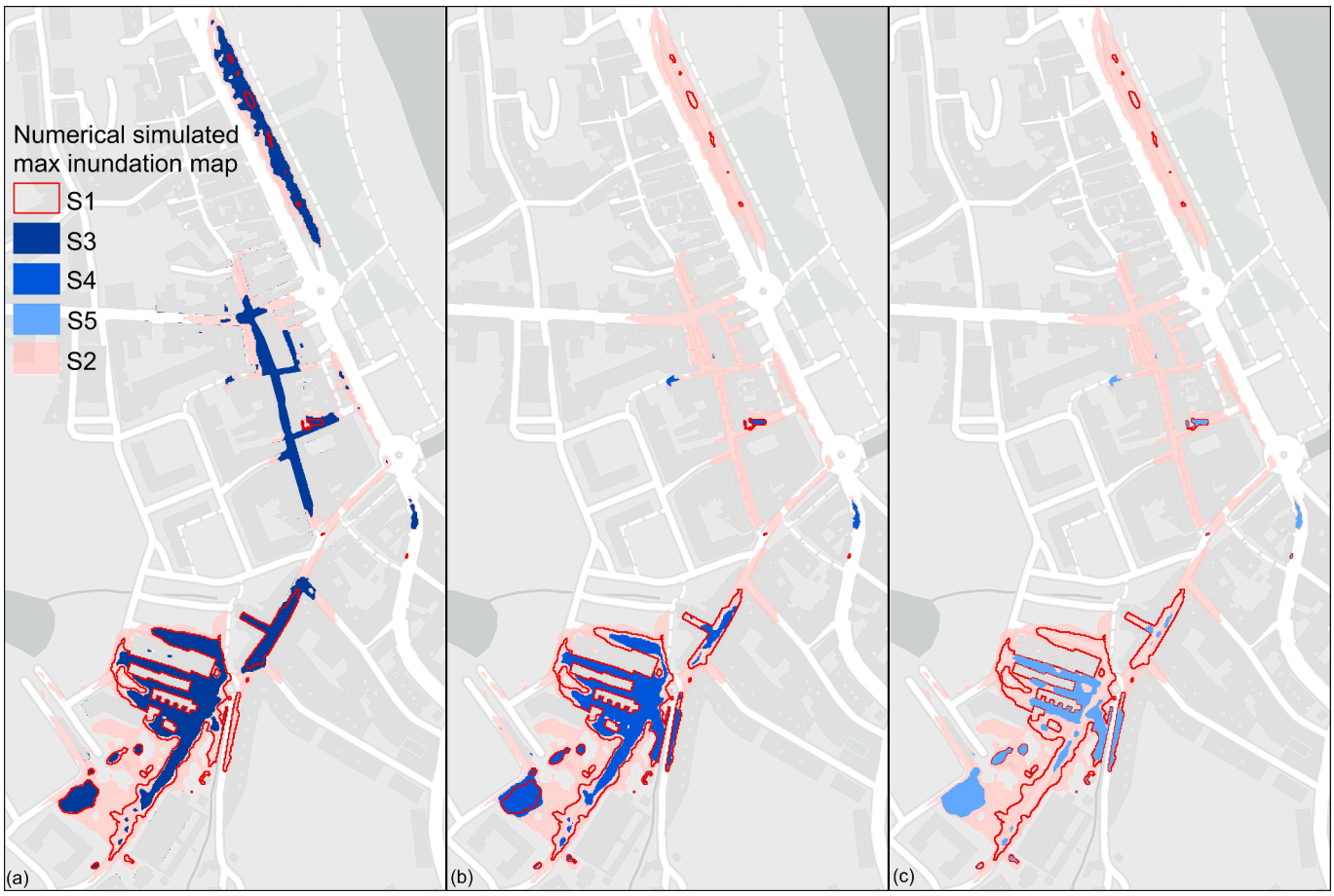

Fig. 8. Numerical simulated maximum inundation extent maps for scenarios S3 (a), S4 (b) and S5 (c) compared with S1 and S2 in the study zones for event E2.

maximum inundation extent, even in extreme scenarios such as E4, which contrasts with the assumptions made by certain authors about the role of the SNDC during extreme rainfall events (Schmitt and Scheid, 2020).

Meanwhile, the application of traditional simplified methods such as those implemented in scenario S3 was also ineffective. In our case study, the SNDC was significantly underestimated in zones 3 and 4 during all four events. This could be attributed to the local topography that facilities runoff accumulation in depressed areas. By contrast, the SNDC was overestimated in events E2 (Fig. 8.a) and E3 (Fig. 9.a) in zones 1 and 2. The main limitation of this methodology seems to be the absence of a physic basis, as it assumes a constant and spatially uniform drainage capacity.

Scenario S4 was shown to be the most effective in the absence of sewer network information. Although its results are not entirely consistent with the reference scenario S1, the performance indices obtained in three of the four analyzed events (E1, E3 and E4) indicate very good model performance, while those obtained in event E2 are acceptable. The differences observed between scenarios S4 and S1 are attributed to the differences between the actual and virtual sewer networks. The virtual network was generated based on current design guidelines, while the actual network might have been designed using older design standards. Typically, current design guidelines tend to be more stringent than older ones. Another reason may be that the actual network is actually a combination of several subnetworks with different outfalls. Due to this, the dimensions of the conduits, i.e., diameters, are smaller than in the virtual network (Fig. 4). Therefore, the SNDC of the real network is smaller than the virtual network, which has a higher water-holding capacity. These reasons which would explain the overestimation of the SNDC observed in zones 1 and 2 during event E2 (Fig. 8.b), and in zone 3 during event E4 (Fig. 10.b). Nevertheless, the virtual sewer network seems to accurately represent the actual sewer network drainage and transport capacity, as well as the flow exchange between the major and minor sewer drainage systems.

Even if scenarios S4 and S5 have the same inlet layout, the maximum inundation map obtained in S5 is less extensive than that in S4. This is because S5 does not include the sewer network, assuming an unlimited capacity of the conduits. Thus, the water entering the inlets is not limited by the hydraulic capacity of the sewers. Similarly, the potential overflows to the surface through manholes when the sewer network capacity is exceeded is not considered. This confirms the significance of using 1D/2D dual drainage models, in that they consider not only the drainage capacity of the network but also the significant flow movement across the major and minor drainage systems.

4.2. *Considerations for the application of the proposed approach*

The application of the proposed approach relies on the generation of a virtual network with realistic features, using an automatic generation tool. The geometry of the network generated for each case study will depend on the characteristics of the study area, such as the topography and local design guidelines. Nevertheless, it is important to inspect certain sections of the virtual network, such as conduct diameters and slopes, or invert depth and invert elevation of manholes, in order to ensure that they exhibit realistic values. Additionally, the spatial information retrieved from OpenStreetMaps and other geodatabases must be verified before its use, in order to prevent potential mismatches with the real urban configuration.

In cases in which information from the real network is available, such as the location of certain network elements like manholes or

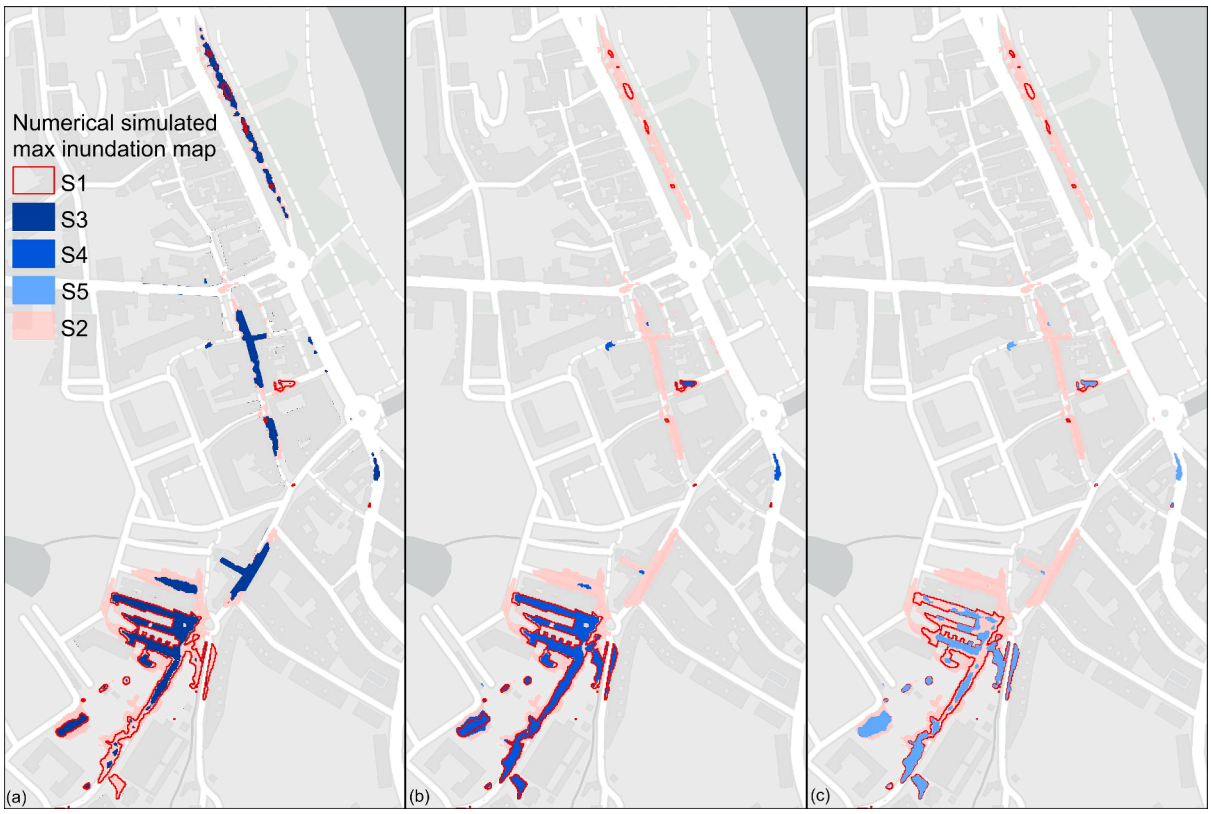

Fig. 9. Numerical simulated maximum inundation extent maps for scenarios S3 (a), S4 (b) and S5 (c) compared with S1 and S2 in the study zones for event E3.

outfalls, or the diameters and arrangement of certain conduits, it can be used to obtain a network more similar to the actual one and therefore, that represents more accurately the sewer network's drainage capacity. The differences between the real network and the virtual network can result in a greater or lesser flood extent. Therefore, attempting to validate the results through the use of satellite images or press reports can contribute to a better performance of the proposed approach.

5. Conclusions

1D/2D dual drainage models have become one of the most useful tools in the assessment of urban pluvial floods. However, these models require detailed information about the sewer network that may not always be readily accessible. This study presented a physics-based approach for assessing urban pluvial floods when detailed sewer network data is not available, and thus overcoming this common issue. The approach uses open-access information within a GIS-Python tool in order to generate a realistic virtual sewer network, based on the high degree of topological correlation between street and sewer network layouts. The virtual sewer network is then used in a 1D/2D dual drainage model, here using the model Iber-SWMM. The proposed methodology was applied to evaluate pluvial flood hazard in a coastal town, focusing on four intense rainfall events, and the results were validated by comparing these with those obtained using the actual sewer network.

The results revealed that the proposed approach can reasonably represent a sewer network's drainage capacity during pluvial floods, especially compared with other simplified approaches, such as the rainfall reduction method, which in the present study significantly underestimated the flood extent, especially in depressed areas. The results confirmed the value of using 1D/2D dual drainage models that consider not only the drainage capacity of the network, but also the interchange of surface runoff across the major and minor drainage systems, and the effect of these processes on the extension of pluvial flooding.

The differences between the results yield by the newly proposed approach and the benchmark are probably explained by the implementation of the current design guidelines in the virtual sewer network generation tool, which may differ from the regulations used during the design of the actual sewer network. Nevertheless, the proposed methodology has been shown to be robust and can be applied when the geometry of the real network is unknown. Consequently, it allows for a realistic identification of areas susceptible to pluvial flooding, regardless of the availability of sewer network information.

Press reports

"*Inundaciones y desbordamientos en la comarca, con 240 litros de lluvia acumulada*" from La Opinión Coruña at https://www.laopinioncoruna.es/gran-coruna/2022/12/26/inundaciones-desbordamientos-comarca-240-litros-80388150.html. "*Sada, uno de los municipios más afectados por las inundaciones*" from La Opinión Coruña at https://www.laopinioncoruna.es/gran-coruna/2022/12/24/sada-municipios-afectados-inundaciones-80370366.html.

CRediT authorship contribution statement

C. Montalvo: Conceptualization, Data curation, Formal analysis, Investigation, Methodology, Writing – original draft, Writing – review & editing. **J.D. Reyes-Silva:** Conceptualization, Software, Supervision. **E. Sañudo:** Conceptualization, Software, Supervision. **L. Cea:** Conceptualization, Funding acquisition, Supervision, Writing – review & editing. **J. Puertas:** Funding acquisition, Supervision, Writing – review & editing.

Declaration of competing interest

The authors declare that they have no known competing financial

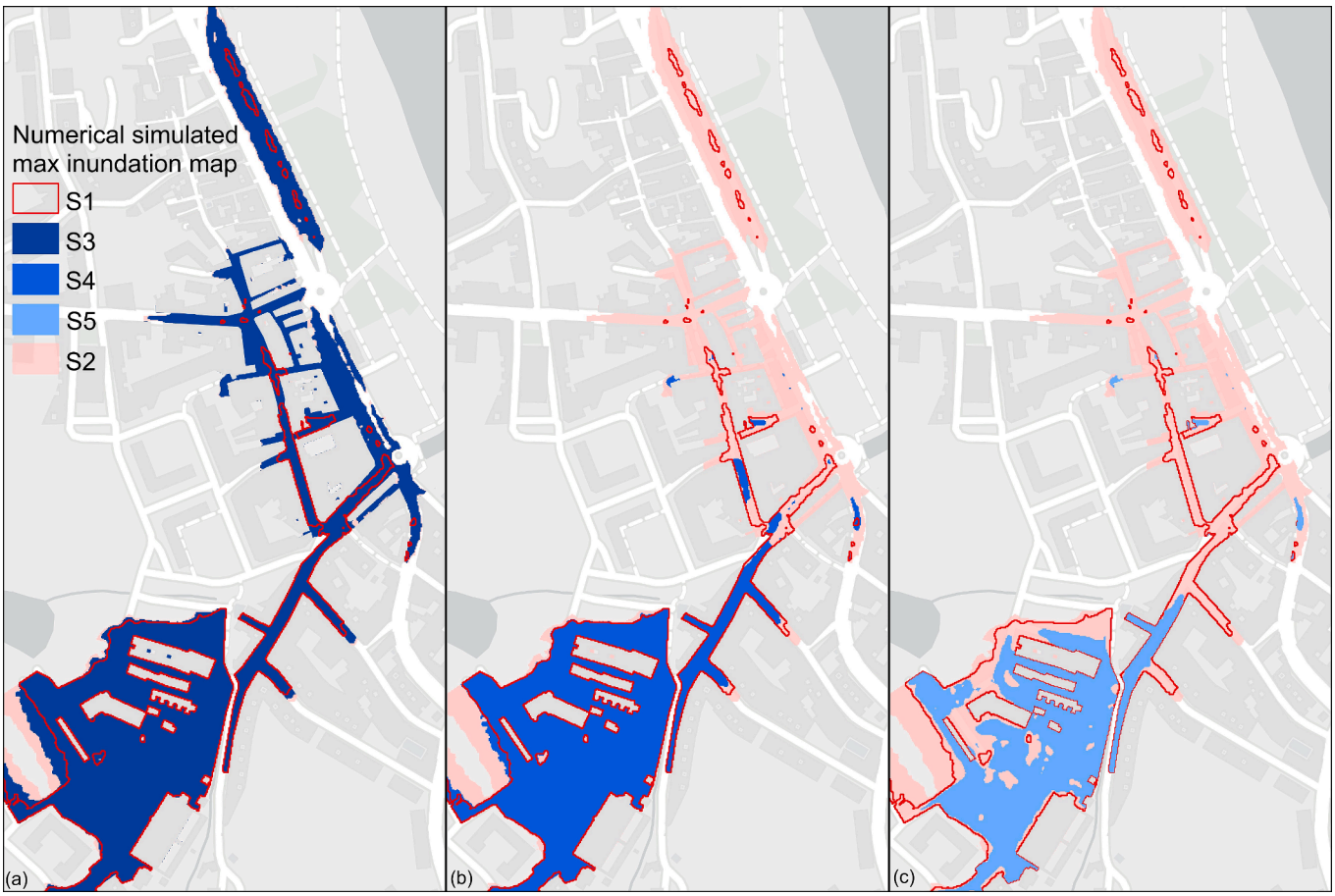

Fig. 10. Numerical simulated maximum inundation extent maps for scenarios S3 (a), S4 (b) and S5 (c) compared with S1 and S2 in the study zones for event E4.

interests or personal relationships that could have appeared to influence the work reported in this paper.

Data availability

Meteorological data were obtained from the agency MeteoGalicia at https://meteogalicia.gal/. Observed sea level data were obtained from the state-owned Spanish Port System at https://www.puertos.es/. The digital elevation model was obtained from the independent Spanish body the National Centre for Geographic Information at https://www.ign.es/. The Soil Conservation Service-Curve Number map was obtained from the Spanish Ministry for Ecological Transition and Demographic Challenges at https://www.miteco.gob.es/. Land Registry, soil use, and population information were obtained from Spanish General Directorate of the Land Registry at https://www.sedecatastro.gob.es/. The street network layout was obtained from the OpenStreetMap geodatabase at https://www.openstreetmap.org/. The LiDAR-derived digital elevation model, observed water elevation data from the gauge station, and the sewer network layout was provided by the regional water administration Augas de Galicia at https://augasdegalicia.xunta.gal/.

Acknowledgments

This project has received financial support from the Spanish Ministry of Science and Innovation (MCIN/AEI/10.13039/501100011033) within the project "SATURNO: Early warning against pluvial flooding in urban areas" (PID2020-118368RB-I00) and the FPI predoctoral grant from the Spanish Ministry of Science, Innovation, and Universities (PRE2021-098425). Funding for open access charge: Universidade da Coruña/CISUG.

References

AdG, A., de Galicia, 2019. Revisión e actualización da avaliación preliminar do Risco de inundación. 2°Ciclo. Demarcación Hidrográfica de Galicia-Costa.

Bennett, N.D., Croke, B.F.W., Guariso, G., Guillaume, J.H.A., Hamilton, S.H., Jakeman, A.J., Marsili-Libelli, S., Newham, L.T.H., Norton, J.P., Perrin, C., Pierce, S. A., Robson, B., Seppelt, R., Voinov, A.A., Fath, B.D., Andreassian, V., 2013. Characterising performance of environmental models. Environ. Model. Softw. 40, 1–20. https://doi.org/10.1016/j.envsoft.2012.09.011.

Bertsch, R., Glenis, V., Kilsby, C., 2017. Urban flood simulation using synthetic storm drain networks. Water (switzerland) 9, 925. https://doi.org/10.3390/W9120925.

Bladé, E., Cea, L., Corestein, G., Escolano, E., Puertas, J., Vázquez-Cendón, E., Dolz, J., Coll, A., 2014. Iber: herramienta de simulación numérica del flujo en ríos. Revista Internacional De Metodos Numericos Para Calculo y Diseno En Ingenieria 30, 1–10. https://doi.org/10.1016/j.rimni.2012.07.004.

Caradot, N., Rouault, P., Clemens, F., Cherqui, F., 2018. Evaluation of uncertainties in sewer condition assessment. Struct. Infrastruct. Eng. 14, 264–273. https://doi.org/10.1080/15732479.2017.1356858.

Cea, L., Álvarez, M., Puertas, J., 2022. Estimation of flood-exposed population in data-scarce regions combining satellite imagery and high resolution hydrological-hydraulic modelling: a case study in the licungo basin (Mozambique). J Hydrol Reg Stud 44, 101247. https://doi.org/10.1016/j.ejrh.2022.101247.

Cea, L., Bladé, E., 2015. A simple and efficient unstructured finite volume scheme for solving the shallow water equations in overland flow applications. Water Resour Res 51, 5464–5486. https://doi.org/10.1002/2014WR016547.

Chen, A.S., Leandro, J., Djordjević, S., 2016. Modelling sewer discharge via displacement of manhole covers during flood events using 1D/2D SIPSON/P-DWave dual drainage simulations. Urban Water J 13, 830–840. https://doi.org/10.1080/1573062X.2015.1041991.

Chow, V.T., 1959. Open-channel hydraulics. McGraw-Hill.

Djordjević, S., Prodanović, D., Maksimović, Č., 1999. An approach to simulation of dual drainage. Water Sci. Technol. 39, 95–103. https://doi.org/10.2166/wst.1999.0451.

Falconer, R.H., Cobby, D., Smyth, P., Astle, G., Dent, J., Golding, B., 2009. Pluvial flooding: new approaches in flood warning, mapping and risk management. J Flood Risk Manag 2, 198–208. https://doi.org/10.1111/j.1753-318X.2009.01034.x.

Ferrer-Julià, M., 2003. Análisis de nuevas Fuentes de datos Para la estimación del parámetro número de curva: perfiles de suelos y teledetección. Centro De Estudios. Hidrográficos.

Fraga, I., Cea, L., Puertas, J., 2017. Validation of a 1D–2D dual drainage model under unsteady part-full and surcharged sewer conditions. Urban Water J 14, 74–84. https://doi.org/10.1080/1573062X.2015.1057180.

García-Alén, G., Hostache, R., Cea, L., Puertas, J., 2023. Joint assimilation of satellite soil moisture and streamflow data for the hydrological application of a two-dimensional shallow water model. J Hydrol (amst) 621, 129667. https://doi.org/10.1016/j.jhydrol.2023.129667.

Grimaldi, S., Li, Y., Pauwels, V.R.N., Walker, J.P., 2016. Remote sensing-derived water extent and level to constrain hydraulic flood forecasting models: opportunities and challenges. Surv Geophys 37, 977–1034. https://doi.org/10.1007/s10712-016-9378-y.

IPCC, 2014. Intergov. panel on climate change 2014 impacts, adaptation, and vulnerability part a: global and sectoral aspects. contribution of working group II to the fifth assessment report of the intergovernmental panel on climate change. Clim. Change.

Jiang, Y., Zevenbergen, C., Ma, Y., 2018. Urban pluvial flooding and stormwater management: a contemporary review of China's challenges and "sponge cities" strategy. Environ Sci Policy. https://doi.org/10.1016/j.envsci.2017.11.016.

Kaspersen, P., Ravn, N., Arnbjerg-Nielsen, K., Madsen, H., Drews, M., 2017. Comparison of the impacts of urban development and climate change on exposing european cities to pluvial flooding. Hydrol Earth Syst Sci 21, 4131–4147. https://doi.org/10.5194/hess-21-4131-2017.

Khaleghian, H., Shan, Y., 2023. Developing a data quality evaluation framework for sewer inspection data. Water (switzerland) 15. https://doi.org/10.3390/w15112043.

Kruskal, J.B., 1956. On the shortest spanning subtree of a graph and the traveling salesman problem. Proc. Am. Math. Soc. 7, 48–50. https://doi.org/10.1090/S0002-9939-1956-0078686-7.

Leandro, J., Chen, A.S., Djordjević, S., Savić, D.A., 2009. Comparison of 1D/1D and 1D/2D coupled (sewer/surface) hydraulic models for urban flood simulation. J. Hydraul. Eng. 135, 495–504. https://doi.org/10.1061/(asce)hy.1943-7900.0000037.

Li, D., Hou, J., Shen, R., Li, B., Tong, Y., Wang, T., 2023. Approximation method for the sewer drainage effect for urban flood modeling in areas without drainage-pipe data. Front Environ Sci 11, 1134985. https://doi.org/10.3389/fenvs.2023.1134985.

Mair, M., Zischg, J., Rauch, W., Sitzenfrei, R., 2017. Where to find water pipes and sewers?-on the correlation of infrastructure networks in the urban environment. Water (switzerland) 9, 146. https://doi.org/10.3390/w9020146.

Martins, R., Leandro, J., Chen, A.S., Djordjević, S., 2017. A comparison of three dual drainage models: shallow water vs local inertial vs diffusive wave. J. Hydroinf. 19, 331–348. https://doi.org/10.2166/hydro.2017.075.

Martins, R., Leandro, J., Djordjević, S., 2018. Influence of sewer network models on urban flood damage assessment based on coupled 1D/2D models. J Flood Risk Manag 11, S717–S728. https://doi.org/10.1111/jfr3.12244.

MOPU, 2016. Ministerio de obras públicas y urbanismo, Norma 5.2 - IC drenaje superficial de la instrucción de carreteras. official state. Gazette.

Moral-Erencia, J.D.D., Bohorquez, P., Jimenez-Ruiz, P.J., Pérez-Latorre, F.J., 2021. Flood hazard mapping with distributed hydrological simulations and remote-sensed slackwater sediments in ungauged basins. Water (switzerland) 13, 3434. https://doi.org/10.3390/w13233434.

Nash, J., Sutcliffe, J., 1970. River flow forecasting through conceptual models part I—A discussion of principles. J Hydrol (amst) 10, 282–290. https://doi.org/10.1016/0022-1694(70)90255-6.

Prokić, M., Savić, S., Pavić, D., 2019. Pluvial flooding in urban areas across the european continent. Geographica Pannonica 23, 216–232. https://doi.org/10.5937/gp23-23508.

Reyes-Silva, J.D., Novoa, D., Helm, B., Krebs, P., 2023. An evaluation framework for urban pluvial flooding based on open-access data. Water (switzerland) 15, 46. https://doi.org/10.3390/w15010046.

Ritter, A., Muñoz-Carpena, R., 2013. Performance evaluation of hydrological models: statistical significance for reducing subjectivity in goodness-of-fit assessments. J Hydrol (amst) 480, 33–45. https://doi.org/10.1016/j.jhydrol.2012.12.004.

Rosenzweig, B.R., McPhillips, L., Chang, H., Cheng, C., Welty, C., Matsler, M., Iwaniec, D., Davidson, C.I., 2018. Pluvial flood risk and opportunities for resilience. WIREs Water 5, e1302.

L.A. Rossman Storm water management model user's manual version 5.1 2015 U.S. EPA.

Salman, B., Salem, O., 2012. Risk assessment of wastewater collection lines using failure models and criticality ratings. J Pipeline Syst Eng Pract 3, 68–76. https://doi.org/10.1061/(asce)ps.1949-1204.0000100.

Sañudo, E., Cea, L., Puertas, J., 2020. Modelling pluvial flooding in urban areas coupling the models iber and SWMM. Water (switzerland) 12, 2647. https://doi.org/10.3390/W12092647.

Sañudo, E., Cea, L., Puertas, J., 2022. Comparison of three different numerical implementations to model rainfall-runoff transformation on roofs. Hydrol Process 36, e14588.

Sanz-Ramos, M., Bladé, E., González-Escalona, F., Olivares, G., Aragón-Hernández, J.L., 2021. Interpreting the manning roughness coefficient in overland flow simulations with coupled hydrological-hydraulic distributed models. Water (switzerland) 13, 3433. https://doi.org/10.3390/w13233433.

Schmitt, T.G., Scheid, C., 2020. Evaluation and communication of pluvial flood risks in urban areas. WIREs Water 7, e1401.

Shi, Z.H., Chen, L.D., Fang, N.F., Qin, D.F., Cai, C.F., 2009. Research on the SCS-CN initial abstraction ratio using rainfall-runoff event analysis in the three gorges area, China. Catena (amst) 77, 1–7. https://doi.org/10.1016/j.catena.2008.11.006.

Tanaka, T., Kiyohara, K., Tachikawa, Y., 2020. Comparison of fluvial and pluvial flood risk curves in urban cities derived from a large ensemble climate simulation dataset: a case study in Nagoya. Japan. J Hydrol (amst) 584, 124706. https://doi.org/10.1016/j.jhydrol.2020.124706.

Wang, Y., Chen, A.S., Fu, G., Djordjević, S., Zhang, C., Savić, D.A., 2018. An integrated framework for high-resolution urban flood modelling considering multiple information sources and urban features. Environ. Model. Softw. 107, 85–95. https://doi.org/10.1016/j.envsoft.2018.06.010.

Xing, Y., Shao, D., Liang, Q., Chen, H., Ma, X., Ullah, I., 2022. Investigation of the drainage loss effects with a street view based drainage calculation method in hydrodynamic modelling of pluvial floods in urbanized area. J Hydrol (amst) 605, 127365. https://doi.org/10.1016/J.JHYDROL.2021.127365.